Meccanica (2021) 56:901–922
https://doi.org/10.1007/s11012-020-01274-3

MODELLING AND ANALYSIS OF MECHANICAL SYSTEMS DYNAMICS

Kinematics of the motorcar body side deformation process during front-to-side vehicle collision and the emergence of a hazard to car occupants

Leon Prochowski · Mirosław Gidlewski · Mateusz Ziubiński · Krzysztof Dziewiecki

Received: 17 March 2020 / Accepted: 15 November 2020 / Published online: 6 January 2021
© The Author(s) 2021

Abstract The kinematics of the process of deformation of the motorcar body side in the culminating phase of a front-to-side vehicle collision has been examined as a possible basis for analyzing and modeling the process of emergence of a hazard to car occupants during a road accident. The course of such accidents has a complex nature and their models are necessarily based on the approximation of non-linear elastoplastic characteristics of impact processes, especially during the transition from the compression phase to the restitution phase of the deformation process. For such characteristics to be obtained, a lot of experimental tests have to be carried out. This paper addresses the short-duration processes with a high degree of complexity.

A front-to-side motorcar collision model has been prepared, which made it possible to analyze the process of deformation of the car body side and the emergence of a hazard and injuries to car occupants. The results of calculation of the deformation rate and range in various car body zones, velocity of the test dummy placed on driver's seat and velocity of possible dummy's impact against the car body side being deformed may be taken as a basis for designing effective occupant protection systems. The kinematics of the phase of vehicle contact and deformation process was modeled with taking into account results of experimental tests, including the curves characterizing the largely non-linear processes that are decisive for the deformation of the car body side. The deformation processes analyzed on these grounds showed at the same time the range of penetration of the deformed body part into the car interior, which causes a hazard to vehicle occupants. The calculation results have shown e.g. that the car body side is deformed to a depth of 0.2 m as quickly as within 0.02–0.03 s. At such a car body side deformation range, the car body part being deformed hits occupant's body in his/her hips and pelvis area with a velocity of about 6 m/s.

Keywords Kinematics of motorcar body deformation · Modeling of front-to-side motorcar collision · Motorcar occupant safety · Deformation rate and range

L. Prochowski · M. Gidlewski (✉)
Military University of Technology (WAT), ŁUKASIEWICZ Research Network – Automotive Industry Institute (ŁUKASIEWICZ–PIMOT), Warsaw, Poland
e-mail: miroslaw.gidlewski@wat.edu.pl

L. Prochowski
e-mail: leon.prochowski@wat.edu.pl

M. Ziubiński
Military University of Technology (WAT), ul. gen. Sylwestra Kaliskiego 2, 01-476 Warszawa, Poland
e-mail: mateusz.ziubinski@wat.edu.pl

K. Dziewiecki
University of Technology and Humanities in Radom, ul. Malczewskiego 29, 26-600 Radom, Poland
e-mail: krzysztof.dziewiecki@uthrad.pl

1 Introduction

The course of the front-to-side collisions, i.e. the collisions where a motor vehicle hits the side of another moving one, is more complicated than that of the head-on collisions. The computational methods and the models that make it possible to analyze the head-on collisions have already become relatively well known. For the front-to-side collisions to be analyzed, instead, models of a higher degree of complexity are required [1]. The current research potentialities enable increasingly extensive use of mathematics, physics and computer technologies for the analysis of motor vehicle collisions. Simultaneously, more in-depth analysis of crash-test experiments becomes possible thanks to employing the new results of studies and research works in the field of experimental mechanics and measurement techniques [2–4]. In consequence, models are being developed thanks to which the methods of minimizing the dynamic loads on vehicle occupants in road accidents may be perfected.

The hazards and injuries to vehicle occupants emerge in result of the action of instantaneous mechanical loads in the culminating phase of vehicle collision. For the process of emergence of such hazards to be analyzed, many other processes, such as e.g. the kinematics of motorcars in the collision phase, including the car body deformation rate in the area of vehicle contact during the collision, must be first known [5]. The information of this kind, obtained by analyzing the course of crash tests, may constitute a good basis for the modeling of the kinematics and dynamics of the process of vehicle body deformation. When such issues are explored, results of measurements of deformations in the vehicle contact zone are usually taken as the starting point. It should be added here that the percentage of the front-to-side collisions under consideration in the total number of vehicle collisions in road traffic shows a rising trend (31.4% in 2018 as against 29% in 2015 [6]).

The hazard associated with the front-to-side collision is bigger than the one posed by the head-on vehicle crash because of much lower energy-absorbing capability of the car body side compared with the vehicle front. In consequence, deep penetration of the deformed car body part into the passenger compartment and high risk of injury caused by its contact with the human body are observed at such accidents [7, 8]. On the other hand, it is well known that the motorcar body construction seriously limits further improvements in the vehicle safety related to side impacts [9].

Although front-to-side vehicle collisions occur quite often, their models still have been insufficiently explored; therefore, the analysis of such accidents is subject to many limitations. In front-to-side collisions, the process of destruction of vehicle bodies includes the interpenetration and 2D or 3D motions of the bodies in relation to each other and this has an impact on the complexity of the models.

Additionally, the uncertainty of data based on different crash tests causes many doubts regarding the validation of the models built in this situation. Hence, a need arises to assess the quality of the data used for the modeling, taken out of necessity from various crash tests. Several stages of such an analysis have been described in publications [10, 11]. Analyses of this kind are carried out with using appropriate analytical or simulation models derived from the theory of mechanics [12].

The analysis of dynamic interactions and their effects, especially the exploration of the dynamic interactions that take place during a collision between motor vehicles, is still an important area of improving and perfecting the methods of modeling and analyzing traffic incidents [13–15]. There are many publications, e.g. [1, 14, 16], dealing with the problems encountered at the modeling and simulation of the motion of solid bodies during the collision phase, especially where not only impact phenomena but also non-linear changes in translational and angular velocities as well as both the compression and restitution phase are taken into account. At present, experimental tests [17] enable more and more detailed exploration of the course of the process of deformation of the motorcar body side and, in consequence, the use of such tests to improve the modeling methods and to minimize the dynamic loads acting on car occupants.

The mathematical model of the motorcar collision describes a few different areas, including reactions and adhesion in the tire-road contact area, hysteresis and damping in the car body deformation process, as well as yaw and lateral displacement in the area of vehicle contact during the collision, the mathematical description of which is quite complicated [18]. In the publications dedicated to side impacts, the calculations are often based upon discrete models

supplemented with empirically determined vehicle deformation characteristics and car body deformations as functions of impacting vehicle's speed. Publications [1, 16] deal with the problems encountered at the modeling and simulation of the motion of solid bodies during the collision phase, especially where not only impact phenomena but also non-linear changes in translational and angular velocities as well as both the compression and restitution phase are taken into account [19].

In the analyses of motor vehicle collisions, the calculations are usually based on discrete dynamic models of the colliding objects. More and more often, they are supplemented with empirically determined vehicle deformation characteristics, parameters of the vehicles involved and dependencies between the empirically determined impacting vehicle's speed and the measured car body deformations [20, 21]. In [10], the analysis of the course of the deformation process in the experimental tests was used to build the model of dynamics of the car collision, which was taken as a basis for determining the forces, displacement and velocities in the area of vehicle contact during the collision. The development of the modeling methods has revealed (see [1, 22]) many difficult scientific problems, which are encountered even when the collisions are described and simulated with using relatively simple discrete systems, especially when not only impact phenomena but also processes of elastoplastic deformation with damping are taken into account.

The development of methods of determining non-linear characteristics of collision processes and the use of such characteristics to build simple models, which are limited by the availability of data collected after a road accident, determinate the objective of the scientific research carried out at many research centers. The complexity of this problem is exemplified by the results of a review of the modeling methods, presented in [18]. Based on this, good points of the simplification of such methods, e.g. by using concentrated parameters and taking into account the action of elastoplastic systems with viscous damping, have been pointed out. It should be added, however, that the modeling of car body deformation characteristics with taking hysteresis into consideration [19] makes it possible to carry out research important for the issues under analysis with taking into account the relations between the course of the characteristic curve and the energy dissipation process at elastoplastic deformations. In the problems of kinematics of motorcar body deformation under analysis, the non-linear characteristics are normally approximated with using the regression methods [1, 16, 22].

The model validation procedure may be treated as the resolving of an "inverse problem" in mechanics, where the course of crash tests is reconstructed on the grounds of the test results with using analytical or simulation models. The validation is based on advanced signal processing techniques, demonstrated e.g. in [13, 14]. An intermediate stage in the validation procedure is the parametric modeling of viscoelastic systems' properties [23, 24], based on the outcome of an approximation of results of measurements carried out during the crash test. The authors are aware of the fact that the models thus built must not be used for the simulation of various collision scenarios because the characteristics that describe non-linear processes only hold in conditions close to those prevailing in the experiment that was taken as a basis for the validation. On the other hand, this method makes it possible to achieve good conformity of model test results with results of experimental tests in the vehicle collision processes, which are very complicated.

The above deliberations about the processes taking place during a front-to-side vehicle collision shows that any analyses of these problems are quite rare in the literature available; therefore, further experimental and model research is necessary.

The objective of this work is to broaden the foundations for analyzing and modeling the process of emergence of a hazard and injuries to motorcar occupants during front-to-side car collisions. The attention has been chiefly focused on enabling reliable modeling of the kinematics of the process of deformation of the car body side and determining the velocity of impact of the car body side being deformed against car occupant's body. The hazard was evaluated on the grounds of the range of deformation of the car body side and the velocity of impact of the car body side being deformed against the occupant's body.

When the data necessary for the modeling were collected, the kinematics of the process of deformation of the car body side was analyzed. With this objective in view, results of crash tests carried out according to two different test procedures were assessed in terms of the usability of such tests for the validation of modeling results.

The improvement of the models is based on results of experimental determination of car body deformation in the culminating phase of the collision. The deformations and forces in the area of contact between the bodies of the car and the car occupant will be modelled with taking into account the non-linear characteristics of different car body areas. With this goal in view, the results of approximating the characteristics of the impact-type process of car body deformation, including the transition from the compression phase to the restitution phase, will be used. An attempt was also made to determine the range of deformation of the car body part penetrating into the passenger compartment and to assess the emergence of a hazard to car occupants. It is worth adding here to substantiate the objective of the research in this field that car's seat belts and front airbags are of little effect (except for preventing the occupant ejection) when the car is struck on its side [25].

This article is an extension of the paper presented at the 15th International Conference "Dynamical Systems – Theory and Applications" DSTA 2019 [26].

2 Crash tests

The information about the deformation processes and hazards arising during road accidents is chiefly obtained from crash test results. The course of such tests represents the most popular types of collisions occurring in road traffic. However, the test results (indispensable for model validation) are scattered and not always adequately described.

During data collection, the available results of conventional front-to-side crash tests and tests carried out to the FMVSS 214 procedure were analyzed. During the conventional front-to-side crash test, both the cars involved are moving (Fig. 1). Such tests (TZ1, TZ2) were carried out at the Łukasiewicz Research Network – Automotive Industry Institute (PIMOT) in Warsaw [10]. The Federal Motor Vehicle Safety Standard (FMVSS) 214 procedure significantly differs from the course of the conventional right-angle crash test [11].

In Fig. 1, the impacting and impacted cars have been denoted by "*A*" and "*B*", respectively. In the FMVSS 214 method, the longitudinal axes of the impacting and impacted vehicles (car *A* and car *B*, respectively) are perpendicular to each other (tests

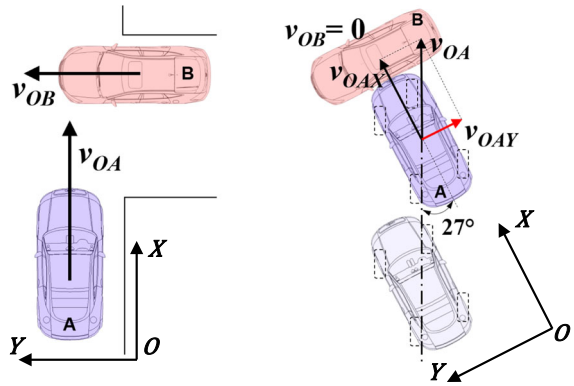

Fig. 1 Conventional right-angle collision (left) and the FMVSS 214 crash test (right), representing such a collision

5146, 5151, 5156, 5161). However, the velocity vector of car *A* is deflected from the longitudinal axis of this vehicle by an angle of 27° (Figs. 1and 2). In the pre-impact phase, car *A* is "crabbing" for the relative motions of both vehicles at the collision instant to be simulated. The FMVSS 214 test results are available from e.g. [17]. Their use for the validation of the computational model of the collision has been considered.

Photographs of the car collision in the TZ1 (conventional) and 5151 (FMVSS 214) tests have been presented in Fig. 2 (see also Tables 1 and 2). They cover the period of up to 150 ms,. The end of the car contact phase of the collision is usually observed to occur at the instant of about 120 ms. In the tests of both types, the pre-impact velocity of car *A* was about 50 km/h. In each of the tests, a Honda Accord car was the impacted vehicle and the course of deformation of its body has been analyzed here.

The substantial differences in the initial conditions of the front-to-side crash tests carried out according to two different procedures raise doubts as to the correctness of any combining or reciprocal supplementing of results of such tests. Therefore, prior to making use of the experimental tests, the complementarity of results of different crash tests was assessed. The following measurement results were considered:

- Time histories of the quantities that describe the kinematics of cars *A* and *B* (as an example, time histories of individual components of the COG velocity vectors of the cars involved, expressed in the global coordinate systems shown in Fig. 1, have been juxtaposed in Fig. 3);

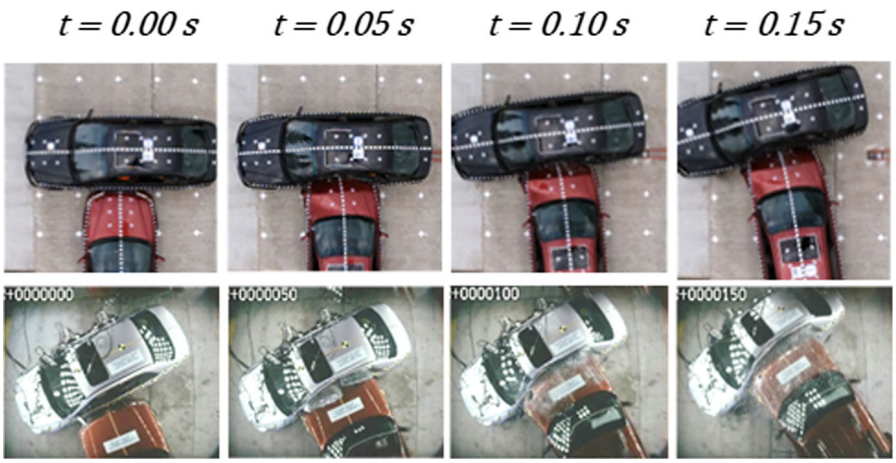

Fig. 2 Successive car positions in the conventional tests (TZ1, top) and FMVSS 214 tests (5151, bottom)

Table 1 Parameters of cars *A*

Test symbol		TZ1A	TZ2A	TZ3A	5146A	5151A	5156A	5161A
Vehicle mass	m [kg]	1 532	1 569	1 569	1 954	2 266	2 347	2 516
Vehicle length	L [m]	4.60	4.60	4.60	4.69	4.80	4.88	5.81
COG (center of gravity) height	h [m]	0.53	0.53	0.53	0.67	0.68	0.70	0.76
Moment of inertia relative to the vertical axis	I_z [kgm^2]	2 636	2 722	2 661	3 587	4 351	4 648	7 065

Table 2 Parameters of cars *B* (Honda Accord), struck on the side of their bodies

Test symbol		TZ1B; TZ2B; TZ3B	5146B…5161B
Vehicle mass	m [kg]	1 568–1 594	1 638–1 642
Vehicle length	L [m]	4.60	4.80
COG height	h [m]	0.53–0.56	0.56
Moment of inertia relative to the vertical axis	Iz [kgm^2]	**2 710–2 827**	3 024–3 031

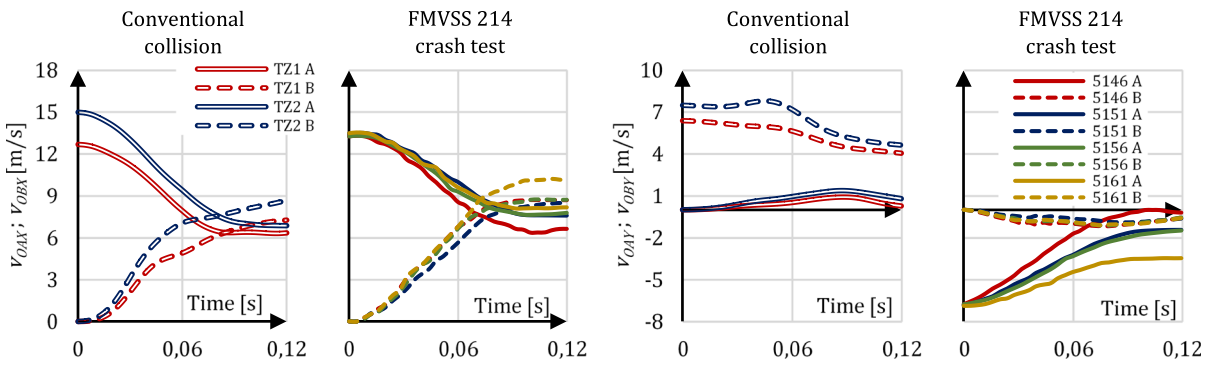

Fig. 3 Example comparison of results of experimental tests carried out to the FMVSS 214 and conventional crash test procedures

- Deformation of the side of bodies of cars B;
- Ttime of duration of the compression phase and the characteristic deformation values at the end of this phase;
- Average car body side deformation vs vehicle velocity curves.

The correlation between the curves obtained from different tests was analyzed and the Pearson's coefficient values were calculated. The results of these calculations carried out for the time histories of individual components of the COG velocity vector of car B (cf. Figures 1and 3) and of the angle and angular velocity of car B body rotation in the OXY plane (yaw, see Fig. 1) have been summarized in Table 3. They show limited similarity between the kinematics of motion of the vehicles in the contact phase of the collision and, in consequence, in the process of deformation of bodies of cars B, i.e. between the behaviors of the impacted vehicles. This has confirmed the doubts as to the correctness of any combining or reciprocal supplementing of the results of tests carried out with using different test methods. Therefore, the validation of the computer model of the collision was based on the making use of results of conventional car crash-test experiments.

3 Model of the front-to-side vehicle collision

The model having been built represents the collision of two vehicles. In the calculational description, both crash test versions under consideration have been taken into account. The vehicle body solids move in a horizontal plane. In the car bodies, the areas that may undergo deformation have been defined. The material points whose motion and dynamic loads correspond to, *inter alia*, the test dummy placed on driver's seat and that are only connected with the car body by non-linear elastoplastic and damping elements have been taken into account as separate objects.

Table 3 Summary of Pearson's coefficient values; the kinematics of cars B

Quantities observed	TZ1B, TZ2B against F214
Velocity v_{OBY}	0.25–0.83
Velocity v_{OBX}	0.97–0.99
Car B body yaw angle	− 0.87 − (+ 0.98)
Car B body yaw velocity	0.16–0.93

The following external forces act in the plane of motion on the car body-dummy system of the Kth vehicle (where $K = A$ for car A and $K = B$ for car B):

- tangent road reaction forces T_{Ki} (i = 1,2,3,4), applied at points of support the tire-road contact areas and acting on the car body via the wheel suspension system, determined experimentally;
- resultant force F of contact between the crashing vehicles, applied at point E (Fig. 4);

The geometry of the car body contour, positions of the points of support *1*, *2*, *3* and *4* in the centers of the tire-road contact areas, position of the center of gravity C_K and the initial dummy's position u_{0mK}, υ_{0mK} have been defined in the local coordinate system $O_K u\upsilon$ attached to the car body solid (Fig. 4).

The test dummy is moving; at any given instant t, it takes the position $\begin{bmatrix} u_{mK} \\ \upsilon_{mK} \end{bmatrix}$ and its velocity relative to the vehicle is $\begin{bmatrix} \dot{u}_{mK} \\ \dot{\upsilon}_{mK} \end{bmatrix}$. It exerts a force $f^m_{pK} = \begin{bmatrix} f^m_{pKu} \\ f^m_{pK\upsilon} \end{bmatrix}$ onto the vehicle and the force exerted by the vehicle onto the dummy has an opposite sense, i.e. it is equal to $f^p_{mK} = -f^m_{pK}$ and is composed of the forces exerted by the seat belt and the seat (Fig. 5).

The forces acting on the dummy are applied to the center of its mass. The forces acting by the dummy on the vehicle exert a moment $M_{f/CK}$ relative to vehicle's center of mass $C_K(u_{C_K}, \upsilon_{C_K})$ (commonly referred to as COG, i.e. center of gravity), where

$$M_{f/C_K} = f^m_{pK\upsilon}(u_{mK} - u_{C_K}) - f^m_{pKu}(\upsilon_{mK} - \upsilon_{C_K}) \quad (1)$$

The following forces are taken into account in the model under consideration, which represents the interaction between the vehicle and the test dummy:

(1) reaction forces exerted by the seat belt and the seat onto dummy's body (spring-damping suspension system acting in the longitudinal direction u with the coefficient of elasticity k_u and viscous damping coefficient b_u and acting in the lateral direction υ with the corresponding coefficients $k_{\upsilon 1}$ and b_υ);

(2) force of dummy's impact against the car body (after the dummy is displaced by a distance of

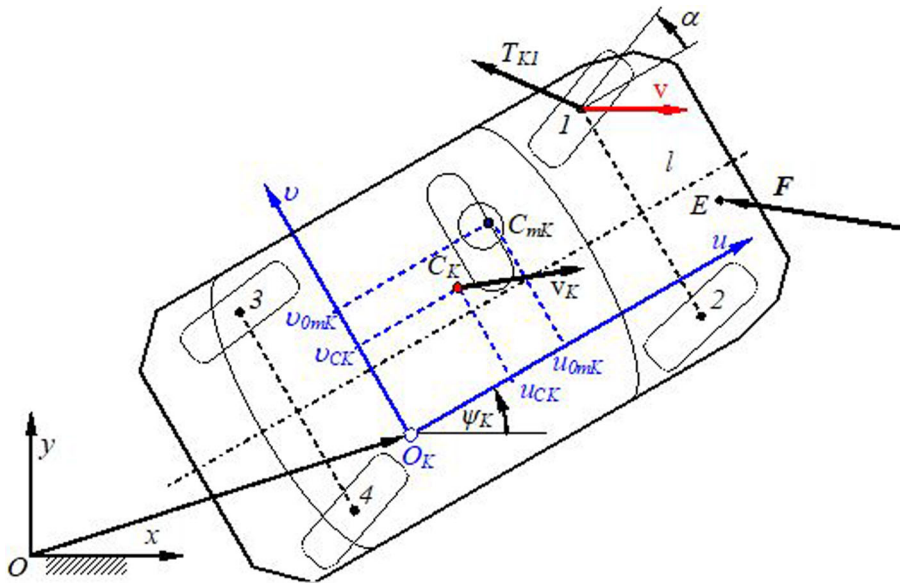

Fig. 4 General physical model of the vehicle with a test dummy: Oxy – global stationary reference frame; $O_K u\upsilon$ – local reference frame, attached to the Kth vehicle

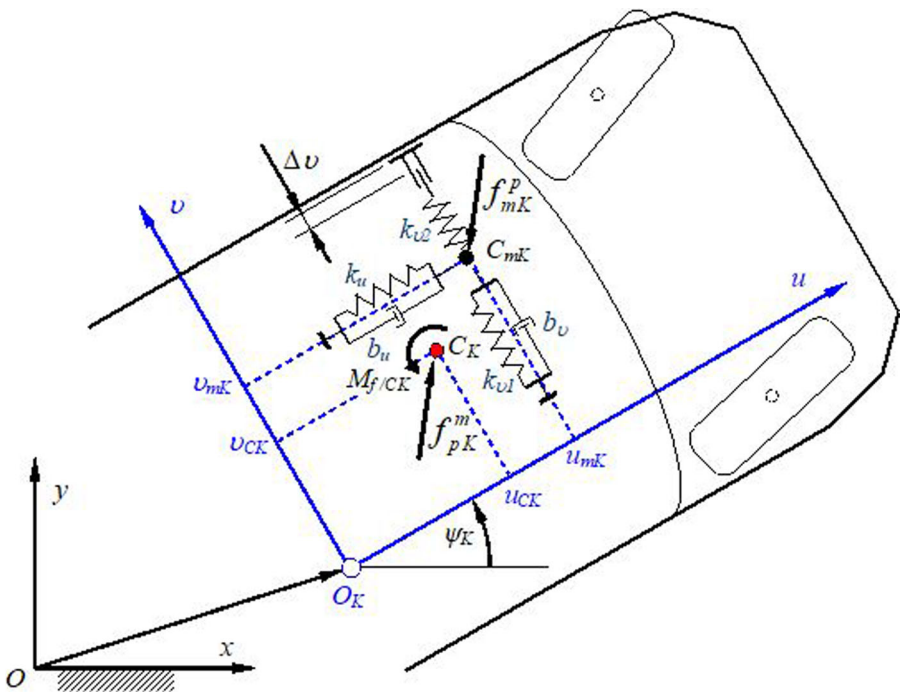

Fig. 5 Model of the interaction between the vehicle and the test dummy

$\Delta\upsilon$, spring $k_{\upsilon 2}$ with an adequately high stiffness is engaged, see Fig. 5).

The position of the vehicle-dummy system is defined by the generalized coordinates expressed in the form

$$q_K = [x_{O_K} \quad | \quad y_{O_K} \quad | \quad \psi_K \quad | \quad u_{mK} \quad | \quad \upsilon_{mK}]^T \tag{2}$$

where: x_{O_K}, y_{O_K}—coordinates of the origin of the local coordinate system in the global system; ψ_K – angular position of the vehicle; u_{m_K}, υ_{m_K}—position of dummy's center of mass in the local coordinate system.

The motion of the vehicle body with the test dummy in the global coordinate system has been described by the following equations:

The motion of the vehicle body with the test dummy has been described by the following equations in the global coordinate system:

$$\begin{aligned} M_K\ddot{x}_{C_K} &= \sum_{i=1}^{4} T_{Kix} + F_x + f_{pKx}^m \\ M_K\ddot{y}_{C_K} &= \sum_{i=1}^{4} T_{Kiy} + F_y + f_{pKy}^m \\ J_{C_K}\ddot{\psi}_K &= \sum_{i=1}^{4} M_{T_{Ki}}/C_K + M_{F/C_K} + M_{f_K}/C_K \\ m_K\ddot{x}_{CmK} &= -f_{pKx}^m \\ m_K\ddot{y}_{CmK} &= -f_{pKy}^m \end{aligned} \tag{3}$$

where:

M_K—vehicle mass, J_{C_K}—vehicle's central moment of inertia, m_K—dummy's mass, $\ddot{x}_{C_K}$, $\ddot{y}_{C_K}$—components of the acceleration of vehicle's COG, $\ddot{\psi}_K$—angular acceleration of the vehicle, T_{Kix}, T_{Kiy}—components of the tangent road reaction acting on the ith wheel, F_x, F_y—components of the reaction force exerted by car B on car A, f_{pKx}^m, f_{pKy}^m—components of the reaction force exerted by the dummy on the car, $M_{T_{Ki}}/C_K$—moment of the ith tangent reaction relative to vehicle's COG, M_{F/C_K}—moment of force F relative to vehicle's COG, M_{f_K}/C_K—moment of force f_{pK}^m relative to the COG of car K (for car B, i.e. where $(K \equiv B)$, the sign of quantities F_x and F_y should be reversed).

Actually, a solution is sought for a system of 10 differential equations (for two motorcars described with Eqs. (3)), where the initial conditions are defined by components of the positions and linear velocities of vehicles' COG, yaw angles and velocities of the cars and components of the positions and linear velocities of the masses that represent the dummies. The numerical computation was carried out in the *Matlab* environment with using the *ode23* procedure with variable integration step. The simulation time was 0.25 s.

The motorcar body is a structure specially formed with particular attention being paid to passive safety. It includes parts (areas) with diverse stiffness, determining the local elastoplastic and damping characteristics that are intended to reduce the effects of a road accident. Experimental test results are available, e.g. in [27], which show the diversity of loads on the car when hitting its front on a rigid barrier. In [28] we can read about the Schaper model, where the car body was divided into zones with different percentage shares in the dissipation of impact energy. Such a division has been logically connected with the deployment of parts with different stiffness in the car body. However, a distinct lack of experiment results that would help in recognizing and describing the properties of a motorcar body side is evident.

Based on the knowledge of design features of energy-absorbing and load-bearing structures and on the available experimental test results, the vehicle body solid in the deformation area (i.e. the body inclusive of all its contents according to the vehicle construction) was hypothetically divided into zones with different elastoplastic and damping properties (Fig. 6). Three zone types were defined for the car front: corner of the car ($A1$), area of location of longitudinal bars characterized by high stiffness ($A2$) and area close to the engine block. In the car side, individual zones were distinguished according to their location, i.e. the areas close to front and rear wheels with their suspension systems ($B1$ and $B7$, respectively), A-pillar ($B2$), front door ($B3$), B-pillar ($B4$), rear door ($B5$) and transition area between rear door and C-pillar ($B6$). The basic dimensions of the individual zones have been specified in Table 4. The resultant force F of contact between the crashing vehicles and the point E of application of this force depend on the elastoplastic and damping properties that have been assumed as assigned to the interpenetrating deformation zones (Fig. 7). The elementary contact forces R (Fig. 7c), generated by the pairs of contacting zones and applied at points $C_{i/j}$ within the area of contact between the zones, determine the range of deformation in the specific zone; having been reduced to the center of mass of the vehicle body, they

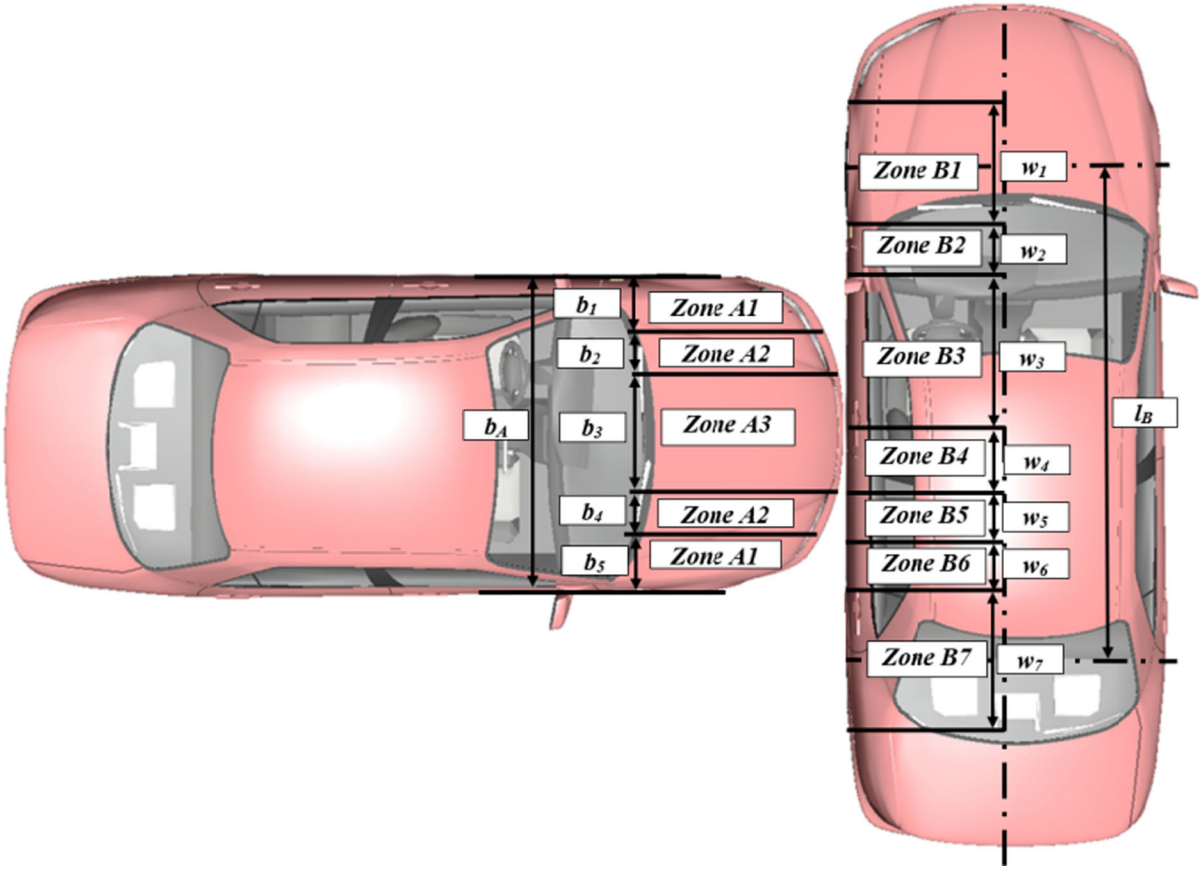

Fig. 6 Location of zones A_i and B_i symbolically marked on the bodies of cars A and B

Table 4 A variant of dimensions of zones A_i and B_i in cars A and B used in tests TZ1

Vehicle A	b_i / b_A (%)	TZ1A	Vehicle B	w_i / l_B (%)	TZ1B (m)
b_A	100	1.750 m	l_B	100	2.675
b_1	15	0.263 m	w_1	33	0.892
b_2	15	0.263 m	w_2	7	0.198
b_3	40	0.700 m	w_3	28	0.743
b_4	15	0.263 m	w_4	9	0.237
b_5	15	0.263 m	w_5	15	0.397
–	–	–	w_6	6	0.148
–	–	–	w_7	33	0.892

are present in the equations of motion (3) of the body as F_x, F_y and M_{F/C_K}.

To calculate the elementary contact forces R between two deformation zones interacting with each other, the following assumptions were adopted (Fig. 7):

1. The zones are convex figures.
2. The tangent direction t-t of the interaction between the zones is parallel to the straight line going through points D_1 and D_2 on the edge of the zones. The normal direction n–n of the interaction is perpendicular to it.
3. The position of points C_i and C_j is defined by the size of the area p of interpenetration of the zones. The contact force R is defined by the deformation

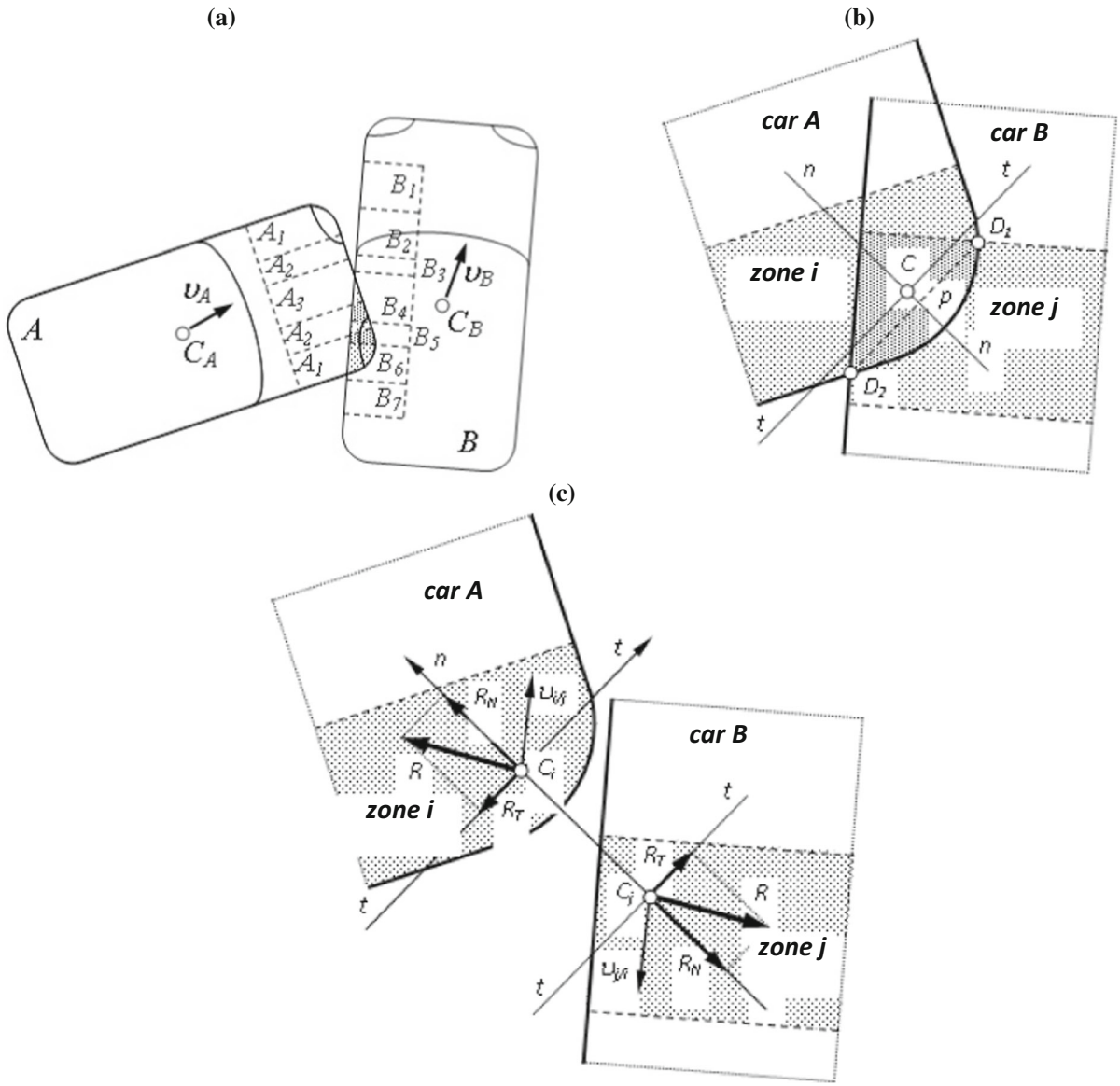

Fig. 7 Area and situation of forces in the area of contact between the interacting car body zones

range and the values of stiffness and damping in the zones and the said values depend on the relation between the non-linear force and the deformation area (Fig. 8). The velocity of point C_i in relation to point C_j, important for the calculation of reaction force R_N, is

$$\vec{\upsilon}_{i/j} = \left[\frac{\upsilon^t_{i/j}}{\upsilon^n_{i/j}}\right] = \vec{\upsilon}_{Ci} - \vec{\upsilon}_{Cj} \tag{4}$$

4. The normal component R_N of the contact force is always a force repulsing the vehicles from each other (Fig. 7c); it depends on the size of the area p of interpenetration of the pair of contacting zones and on the relative normal velocity $\upsilon^n_{i/j}$ of the zones

$$R_N\left(p,\, \upsilon^n_{i/j}\right) = R_N(p) + R_N\left(\upsilon_{i/j}{}^n\right) \tag{5}$$

5. The tangent component of the contact force

$$R_T = \mu_{ij} R_N \tag{6}$$

is always so directed that it counteracts the sliding of the zones in relation to each other and the coefficient of kinetic friction μ_{ij} may be a function of the relative velocity $\upsilon^t_{i/j}$ of points in the tangent direction (Fig. 7c).

The force $R(R_N, R_T)$ in Fig. 7c represents the interaction within individual pairs of deformation zones of the bodies of cars A and B. The forces denoted by F in the equations of the collision model are resultants of the forces R that simultaneously act within a number of pairs of the deformation zones being in contact during the collision (shown in Fig. 6).

4 Non-linear characteristics of the deformation process

The curves characterizing the non-linear deformation were determined from results of crash tests with a frontal car impact against a rigid barrier (NHTSA, car A [17]) and with a front-to-side car collision (Ł-PIMOT, car B [10]), carried out with various speeds within a range of 40–55 km/h. Then, the curves characterizing the deformation, plotted for various impact speeds, were approximated by polynomial functions and the curves thus obtained were used in simulation tests of front-to-side car collision with car A speeds ranging from 40 to 65 km/h. Figure 8 shows examples of the deformation characteristics of a few body zones of cars A subjected to tests TZ1 and TZ2 (for the zone symbols used see Figs. 6 and 7a). The shapes of these curves show great diversity depending on the position of individual zones in the car body.

While example results of testing the deformation of the motorcar body front are available [17], there is a lack of data describing the characteristics of the car body side. Therefore, to assess the hazard to car occupants, the lacking curves characterizing the deformation of similar zones in the car B body side were roughly determined from crash test results [10].

Based on the curves characterizing the deformation in the compression phase, the course of the dynamic deformation during the crash test and the static deformation after the crash test completion, models representing these characteristics were prepared. Examples of the model curves have been shown in Fig. 9 and the calculational description with the compression and restitution phase being represented separately has been given below.

$P_k(p_k; R_{Nk})$ point representing the end of the compression phase;

$P_r(p_r; 0)$ point representing the end of the restitution phase on the dynamic deformation curve;

$P_{st}(p_{st}; 0)$ value of the permanent (static) car body deformation in the zone under analysis.

The curves characterizing the deformation in the compression phase were approximated by polynomial as follows:

$$R_N(p) = k_1 p^3 + k_2 p^2 + k_3 p; p \in (0 \rightarrow p_k) \tag{7}$$

where: k_1, k_2, k_3—coefficients of the approximating polynomial, obtained by the least squares method.

The restitution phase was represented by a parabola

$$R_N(p) = r_1 p^2 + r_2; \mathrm{p} \in (p_k \rightarrow p_r) \tag{8}$$

$$r_1 = \frac{R_{Nk}}{2p_k p_{sp} - p_{sp}^2}; r_2 = \frac{-R_{Nk}(p_k - p_{sp})^2}{2p_k p_{sp} - p_{sp}^2} \tag{9}$$

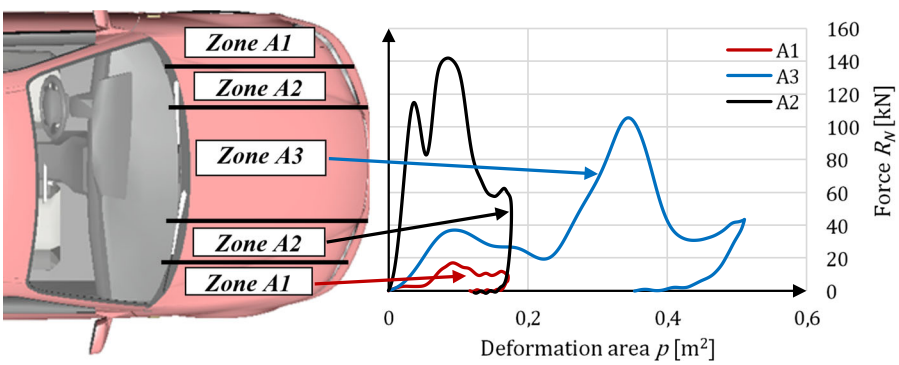

Fig. 8 Non-linear characteristics of the zones of deformation of the car body front during the compression and restitution phase

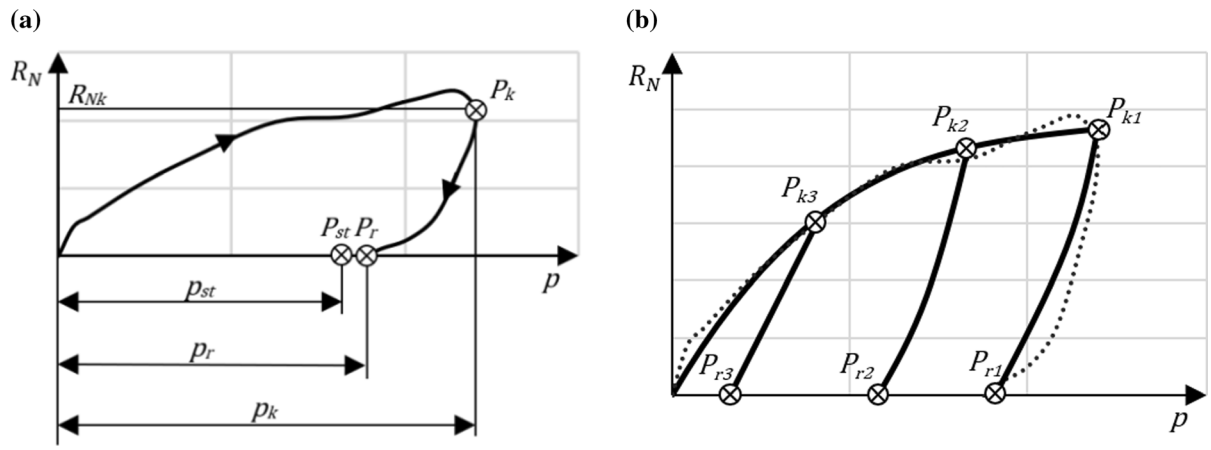

Fig. 9 The example of the car body deformation characteristic and its approximation: **a** actual curve based on experimental research; **b** approximation of the curve, showing the deformation in the restitution phase for various positions of the point representing the end of the compression phase

which goes through points $P_k(p_k, 0)$, $P_r(p_r, 0)$ and $-P_r(-p_r, 0)$ (Fig. 9). In the modeling, the point of transition from the compression to restitution phase was assumed as the instant in the collision time when the distance between the centers of mass of car A and B bodies reached its minimum.

Apart from summand $R_N(p)$, Eq. (5) includes a term $R_N(v^n_{i/j})$. Its physical sense is connected with the energy dissipation during the deformation of car bodies. However, the separation of the compression and restitution phase from each other in the motorcar collision process, followed by diversification of the functional dependence $R_N(p)$ in these phases (Eqs. (7), (8) and (9)), makes it possible to represent the elastoplastic process of the collision. Therefore, in the calculation example considered in this study an assumption was adopted that $R_N(v^n_{i/j}) = 0$. In such an approach, the value of the normal force R_N actually depends on the deformation area only, but this dependence is different for the compression and restitution phase.

For the approximation of the experimental test results, the available descriptions of the elastoplastic properties of car bodies [29–31] were used. The experimental test results [32, 33] clearly show the non-linear properties of car bodies in terms of deformations caused by impact loads (cf. Figure 8). The use of a third-degree polynomial ensured high accuracy of such an approximation (for correlation coefficient values being used as an indicator).

Parameter p_{sp} defines the share of elastic deformations in the dynamic deformation of the car body. Its value depends on the value of p_k, i.e. $p_{sp} = f(p_k)$; the type of this dependence was determined from the values of p_r and p_{st} (cf. Figure 9).

The graphical characteristics of the zones of deformation, exemplified in Fig. 8, were used for determining the $R_N(p, v^n_{i/j})$ and $R_T(R_N)$ curves (Eqs. (5) and (6)). The necessary static deformation values were determined by measurements of the crash-tested car bodies. The experimental test results (cf. Figure 3) were taken as a basis for determining the car body deformation rate. In consequence, the determination of the time history of this rate made it possible to relate this rate to the test dummy impact velocity in the deformation zone.

The graphical deformation characteristics $R_N(p, v^n_{i/j})$ shown in Figs. 8 and 9 describe the properties of individual deformation zones in the bodies of cars A and B. During a collision, interaction between these zones takes place. Therefore, an equivalent characteristic curve $R_{Nij}(p_{ij}, v^n_{i/j})$ must be determined, from the deformation characteristics $R_{Ni}(p_i, v^n_{i/j})$ for the ith zone of car A and $R_{Nj}(p_j, v^n_{i/j})$ for the jth zone of car B, to determine the values of the contact forces between the pairs of zones having common areas p of interpenetration.

5 Validation of the model

The model parameters were categorized as those measurable (e.g. mass and inertia data, geometrical dimensions), computable (e.g. elastoplastic characteristics of the front car body part, forces of the resistance to motion) and having to be estimated (i.e. the data that describe the elastoplastic and damping characteristics of individual zones in the car body side). In the model validation process, attention was focused on the parametrization of the data of the third category. A validation procedure was developed, which was taken in part from works [30, 34, 35]. The parameter values sought were estimated, as a basis, from experimental test results and then simulation calculations were carried out on these grounds. The calculation results were compared with results of experimental tests. Some physical quantities describing the kinematics of the car struck on its side were assessed. This constituted the first stage of the model validation process. Afterwards, numerical tests were planned and carried out, where the model sensitivity to the values of the parameters estimated was checked. The model was found to be considerably sensitive to the parameters describing the elastoplastic properties of individual zones in the car body side. In this connection, attention was focused on the adequate selection of these data in the further validation process. The conformity of the modeling results with the results of experimental tests was assessed. Comparisons were made between the quantities that are decisive for the kinematics of the deformation process, i.e. time histories of the car body yaw angles (ψ_A and ψ_B), components of linear COG velocity vectors and angular (yaw) velocities ($\dot{x}_{CA}, \dot{y}_{CA}, \dot{\psi}_A, \dot{x}_{CB}, \dot{y}_{CB}, \dot{\psi}_B$), as well as components of COG acceleration vectors ($\ddot{x}_{CA}, \ddot{y}_{CA}, \ddot{x}_{CB}, \ddot{y}_{CB}$) of cars A and B during the contact phase of the collision. As a conformity assessment criterion, the value of the coefficient of linear correlation was adopted.

Figure 10 shows the result of identification of the elastoplastic characteristics of individual zones in the car B body side, which are described by functions $R_{Ni}(p_i, v^n_{i/j})$ (Fig. 10a) and the dependence of force R_N on linear deformation c of the car B body, with $c_i = p_i/w_i$, where w_i is the width of the ith zone in the car body side (cf. Figure 6 and Table 4). The deformation curves presented in Fig. 10b show a great diversity in the properties of individual zones in the car B body side. This means that the car body side features protecting the passenger compartment from penetration of car body parts vary a lot.

Figure 11 shows the outcome of comparing the results of experimental and model tests. The results of model simulation of cars' motion during the contact phase of the collision were found to be consistent with results of experimental tests, which provided grounds for the starting of model research related to the subject matter of this work.

6 Model test results and discussion

At the first stage of this research, a collision of the cars in conditions identical to those of test TZ1 (V_{A-} = 46 km/h, V_B = 23 km/h) and test TZ2 (V_{A-} = 55 km/h, V_B = 27 km/h) was simulated. Time histories of the following quantities, considered important for the analysis of hazards to vehicle occupants but difficult to be obtained experimentally, were determined:

- Elementary contact forces R_N generated in the interpenetrating deformation zones during the collision (Fig. 12—test TZ1); these forces were decisive for the shape and range of deformation in a specific zone;
- Areas p and deformation ranges c in individual deformation zones (Fig. 13—test TZ1), i.e. the effect of action of forces R_N (presented in Fig. 12);
- Deformation growth rates in individual deformation zones of the car body side (Fig. 14—test TZ1), calculated with using the process of growth of the deformation area, shown before (Fig. 13);
- Lateral component of the velocity of the test dummy placed on driver's seat, juxtaposed with the deformation growth rate of the car body side, translating into the velocity of displacement of the car body panel (Fig. 15—test TZ1, example for zone 3); in the car, the zone was chosen that corresponds to the location of driver's door and seat.

The analysis of the simulation test results has been focused on the kinematics of the process of deformation of the car body side. The depth of the deformation (i.e. of the car body penetration into the passenger compartment) and the velocity of impact against the

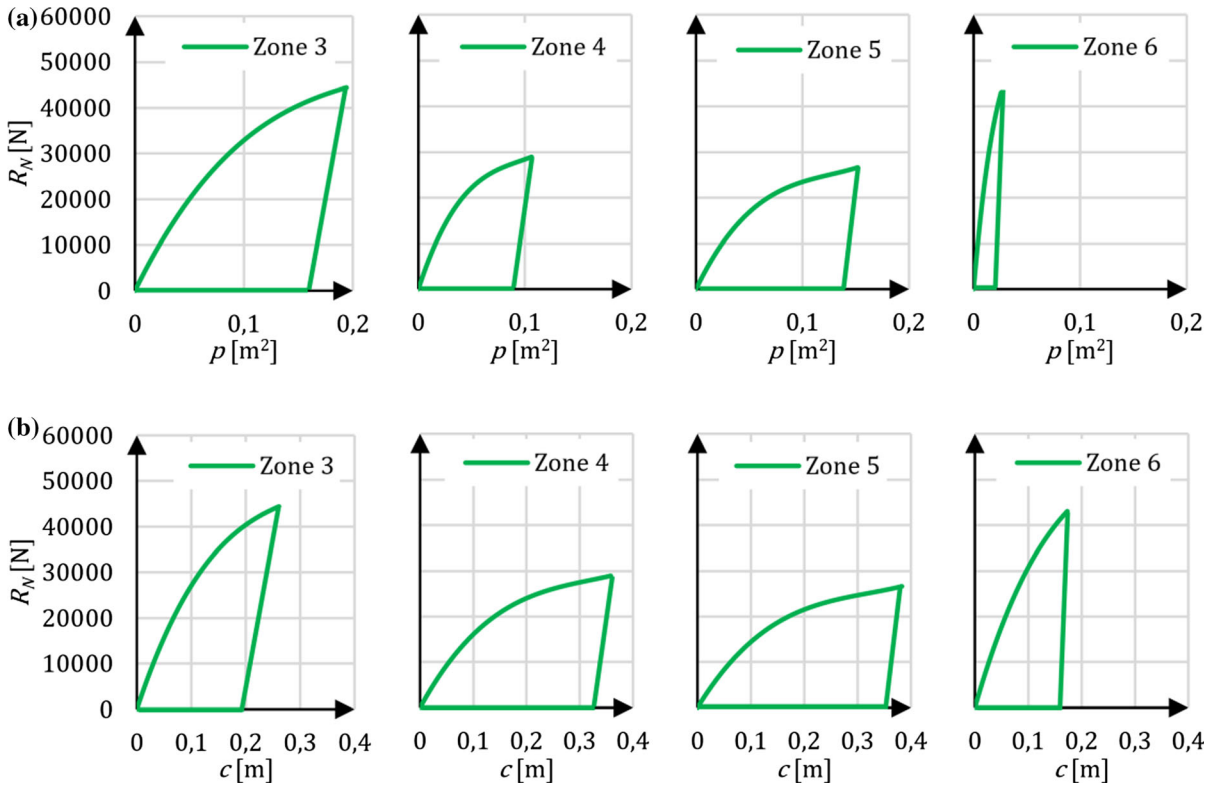

Fig. 10 Deformation characteristics of individual deformable zones in the car B body side

side of car occupant's body are of critical importance for the emerging hazard and injuries and for the designing of a passenger protection system. The motorcar collision model having been built makes it possible to define the hazard factors mentioned above and their dependence on vehicle properties and pre-impact speed.

Figures. 12and 13 show time histories of the deforming force and the deformation range in zones 3, 4, 5 and 6, where the car body side was significantly deformed. The calculation results presented in Figs. 13 and 14 show the kinematics of the car body side deformation process in individual deformation zones and make it possible to determine deformation characteristics of the deformed zones of the side of car *B*. Time histories of the velocity of deformation calculated for individual zones in the car *B* body side (Fig. 14) analyzed together with time histories of the velocity of dummy's motion towards the car body side being deformed enable precise determination of the impact energy and the place of impact on the contour of car occupant's body. Results of such calculations have been shown as an example in Fig. 15. The calculations were carried out for zone 3, which corresponds to the location of driver's door and seat and driver's hips.

At the next stage, the influence of the pre-impact speed of car *A* on the kinematics of the process of deformation of car *B* body side (Figs. 16, 17 and 18) and on the process of generation of a hazard that the driver would be struck on his/her side was examined. At present, the research on the influence of the side impact speed on the generation of injuries is often analyzed [36–38], e.g. from the point of view of the assessment of risk in road accidents. In the tests under consideration, the speed of the impacting car (*A*) was 40, 45, 50, 55, 60 and 65 km/h; car *B* moved with a speed of about 24 km/h.

The contour of the deformation of car *B* body side at the end of the compression phase has been outlined in Fig. 16 for a few values of the impact speed of car *A*. To define the contour of deformation of the car *B* body side, points *P*1…*P*7 were used, which were situated in the middle of the width of each of the

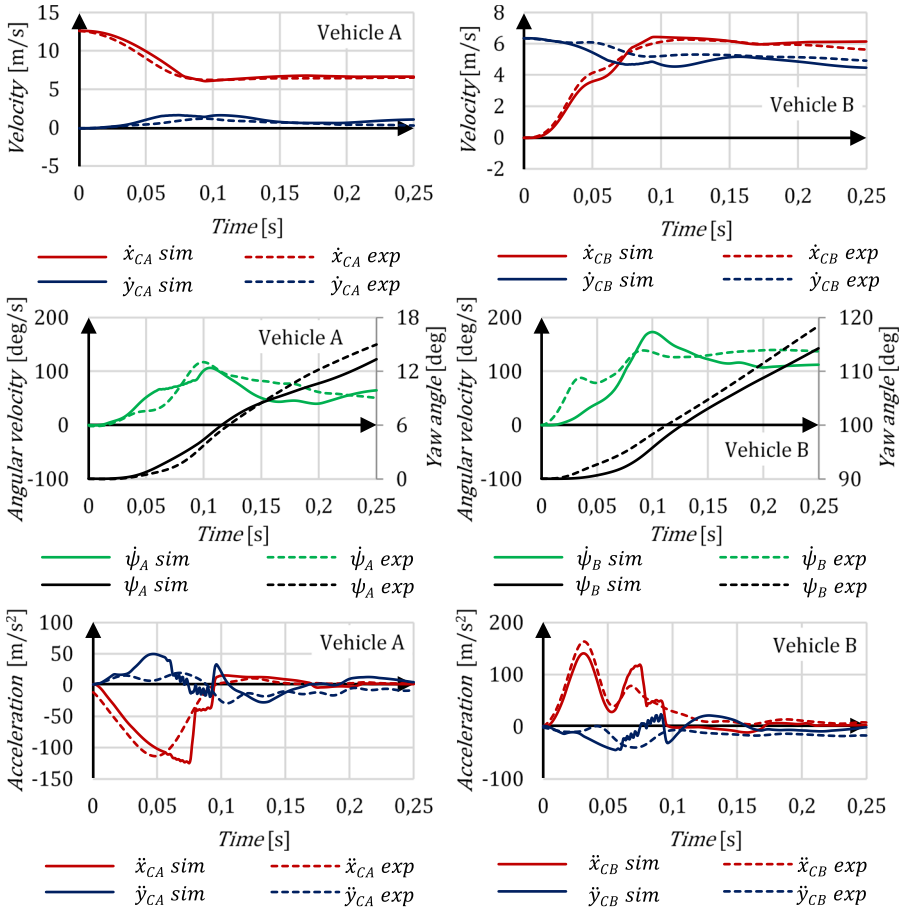

Fig. 11 Time histories of angular displacements, linear and angular velocities and accelerations of car bodies in the contact phase of the collision of cars *A* and *B*; example for the cars subjected to test TZ1

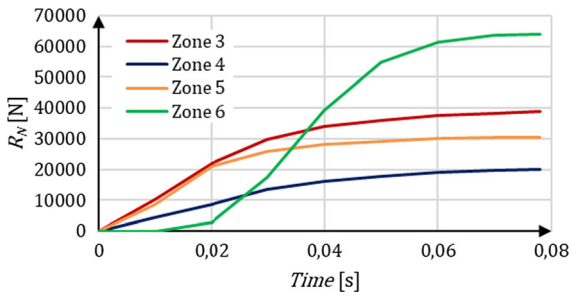

Fig. 12 Time histories of forces R_N in the car *B* body side zones that were deformed during the collision

deformation zones adopted. The lateral displacements of these points show the deformation in individual zones. Time histories of the deformation and deformation rates in individual zones (showing, in consequence, changes in the positions of points P_i in relation to the coordinate system attached to car *B*) for different values of the impact speed of car *A* have been brought together in Fig. 17. The curves plotted with heavy lines apply to point *P*3 as the one representing the car body area that may hit the car occupant. The kinematics of deformation (displacement) of individual points on the car body side as a function of the velocity of impact of car *A* against the side of car *B* has been presented in Fig. 18.

The velocity of impact of human occupant's body against the car *B* body side being deformed at a front-to-side collision with an impacting car's speed of about 50 km/h is as high as 6 m/s. The time histories of the deformation rate of the car body side and the lateral dummy's velocity obtained from the simulation were in conformity with the course of the (Figs. 19 and 20) experimental tests where the impact of car body side against occupant's body was observed. The passive safety systems provided in the car protect, first

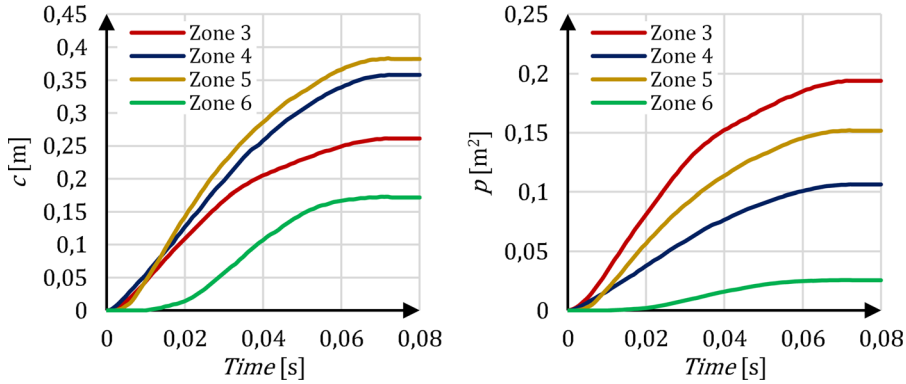

Fig. 13 Time histories of the area p and deformation range c in the car B body side zones that were deformed during the collision

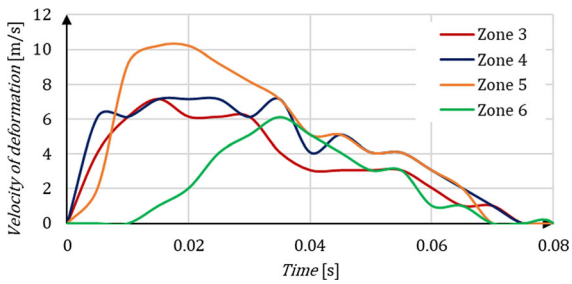

Fig. 14 Deformation growth rates (velocities) in a few successive zones of the car B body side during the collision

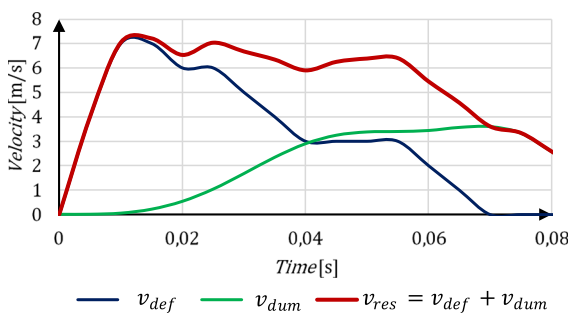

Fig. 15 Time histories of the rate (velocity) of deformation of the car body side in zone 3 (v_{def}), dummy's velocity (v_{dum}) and velocity of dummy's impact against the car body side being deformed (v_{res})

of all, occupant's head and chest area; actually, however, the hips and pelvis of the occupant are usually struck due to excessive deformation of the car body side.

The front-to-side car collision model having been developed has made it possible to determine characteristics of car body side deformation, deformation range and deformation rate for various areas in the car body side as well as characteristics of the velocities of the test dummy placed in driver's seat and of the possible dummy's impact against the car body side being deformed during the accident. The dynamic car body deformation and non-linear characteristics of the transition from the compression to restitution phase of the deformation, regardless of the deformation range, have been taken into account in the model. The test results presented as an example confirm the possibility of carrying out extensive model tests with taking into account various properties of the car bodies, various pre-impact speeds of car A and various positions of car B driver and passengers relative to the car body side. The results of such tests will be used to forecast the bodily injuries to the car occupants in road accidents of this type and will constitute a basis for designing new systems of passenger protection in front-to-side vehicle collisions.

7 Summary and conclusions

The validation test results have confirmed the model properties to be in conformity with crash test results. This makes it possible to carry out reliable simulations of the process of motorcar collisions and deformation of the impacted car's body side.

Before being used in the model validation process, the collected results of experimental research including crash tests carried out according to two different

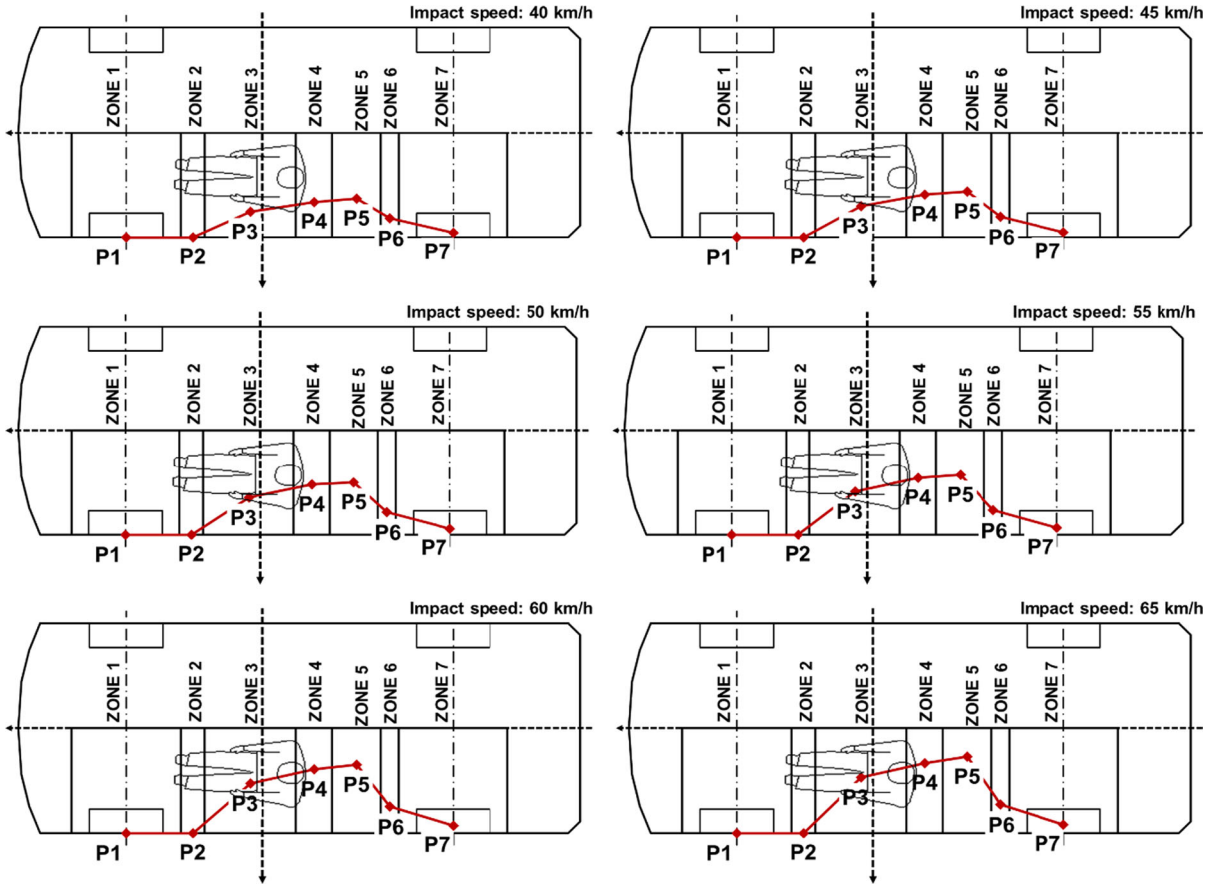

Fig. 16 Contour of the dynamic deformation of car *B* body side (at the end of the compression phase) for different values of the impact speed of car *A*

methods were subjected to conformity assessment based on Pearson's coefficient values. The calculation results have revealed the necessity of exercising great caution when combining data obtained from different crash tests. For the model validation, only results of crash tests carried out to the conventional method were used. The motorcar collision model having been built makes it possible to examine the hazard creation processes and the dependence of the hazard on vehicle properties and pre-impact speed. In particular, the following has been ascertained:

- The model developed to represent the car body side (within the area between the front and rear wheel) and the proposed division of the car body side into 6 zones with diverse stiffness (Fig. 6, Table 4) offers high conformity of the kinematics of the motorcar body deformation process with that observed in crash tests carried out on medium-size cars with the sedan-type body.
- The approximation of the non-linear characteristic curve representing the elastoplastic properties of the car body side (Fig. 9) by a third-degree

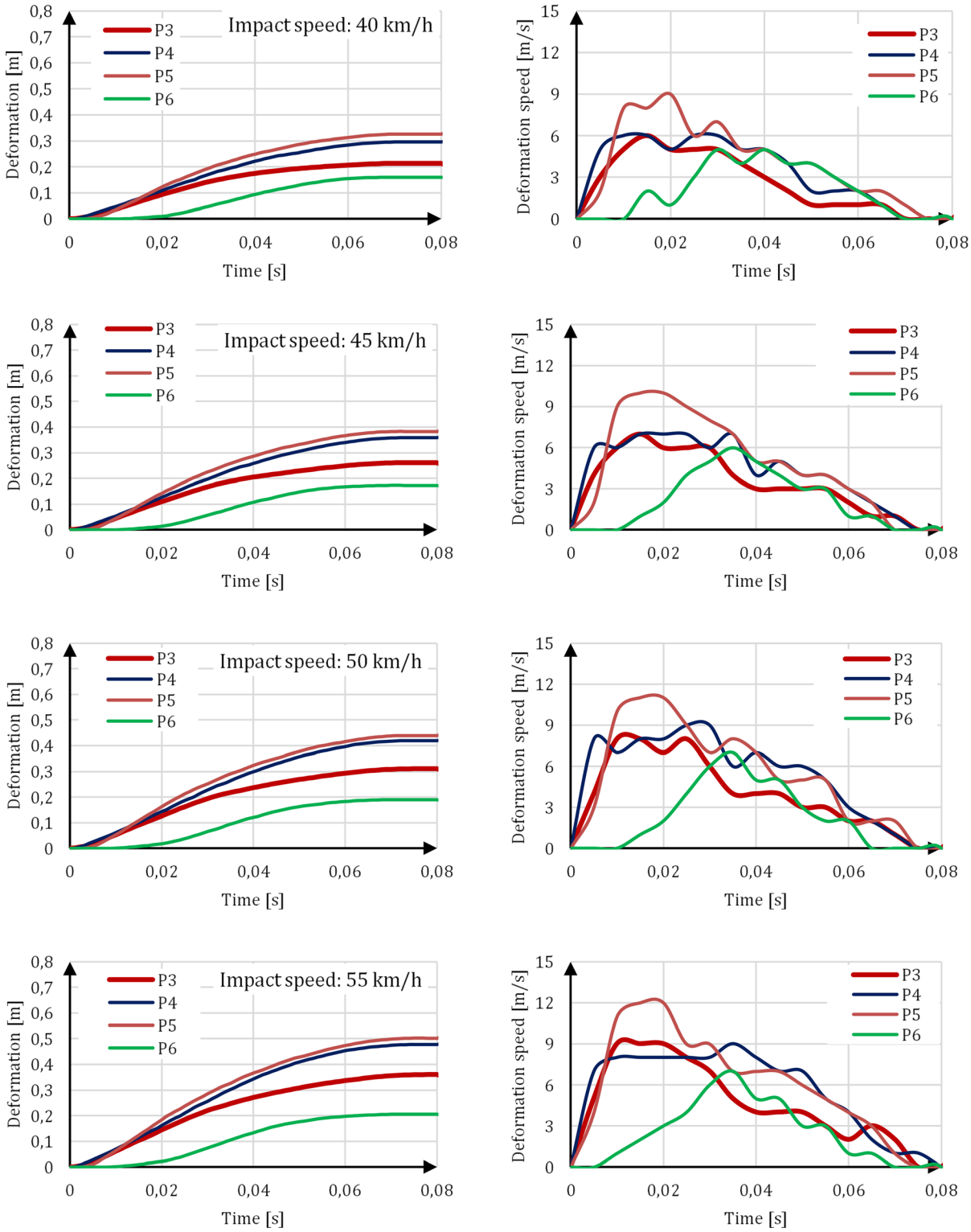

Fig. 17 Time histories of the deformation and deformation rates in individual zones in the car *B* body side for a few values of the impact speed of car *A*

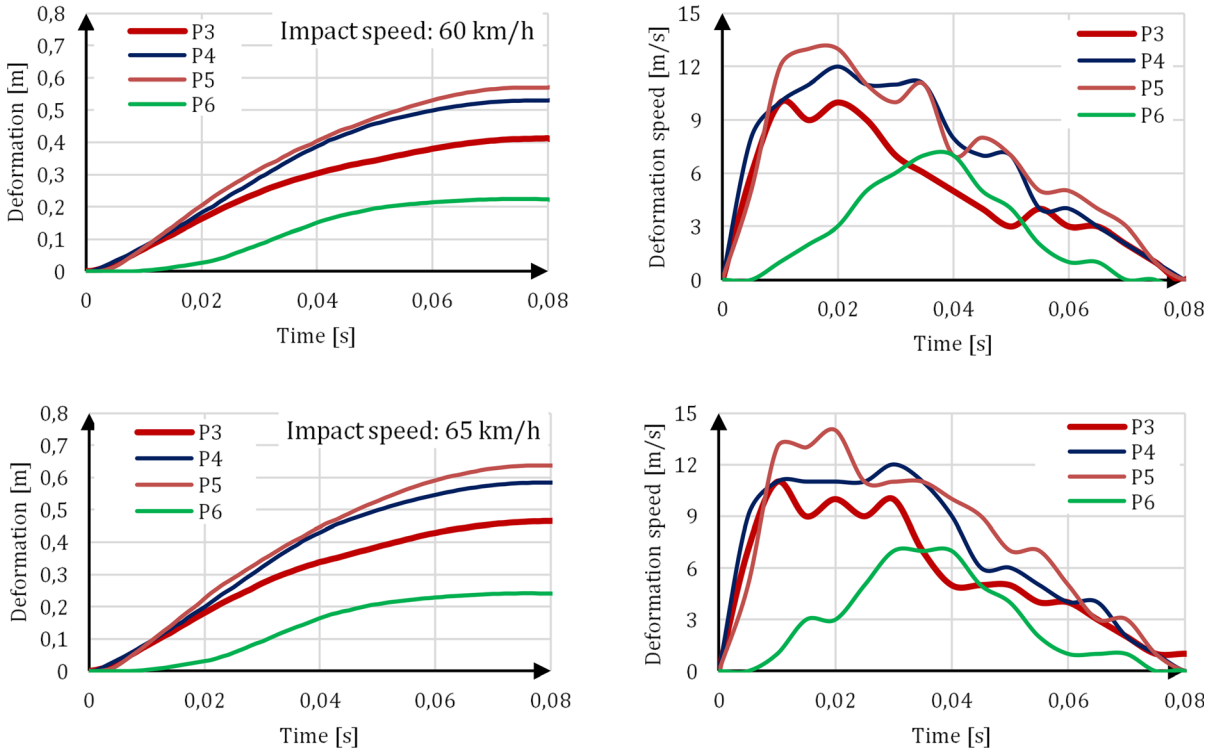

Fig. 17 continued

polynomial and an inverted parabola (Fig. 10 and (Eqs. (7), (8), (9)) makes it possible to obtain a reliable contour of the body side deformation in the compression and restitution phase during the front-to-side motorcar collision.

- The car body side deformation capable to cause an impact against car occupant's hips occurs as quickly as after 0.02–0.025 s from the beginning of the collision (Figs. 17, 18), i.e. within a time shorter than that observed at the frontal impact against an obstacle; this also defines the time available for a defensive reaction of a passive safety system provided at the car body side.
- In the zone of maximum deformation (Fig. 6), the car body side hits occupant's hips with a velocity of 7 m/s after 0.01 s from the beginning of the collision (Fig. 15).

The diversity in the non-linear characteristics of car body side deformation, shown in Fig. 13 and the deformation rate curves (Fig. 14) indicates strong interrelation between the collision effects, i.e. the dynamic loads acting on car occupants, the kinematics of the car body deformation processes observed and the car body properties. The determination of this diversity enables the authors to explore the possibilities of minimizing the risk of injuries depending on the properties of the energy-absorbing zones in the car body side. The model having been built provides a computing potential that makes a basis for designing car body structures with new properties and new car occupant protection systems.

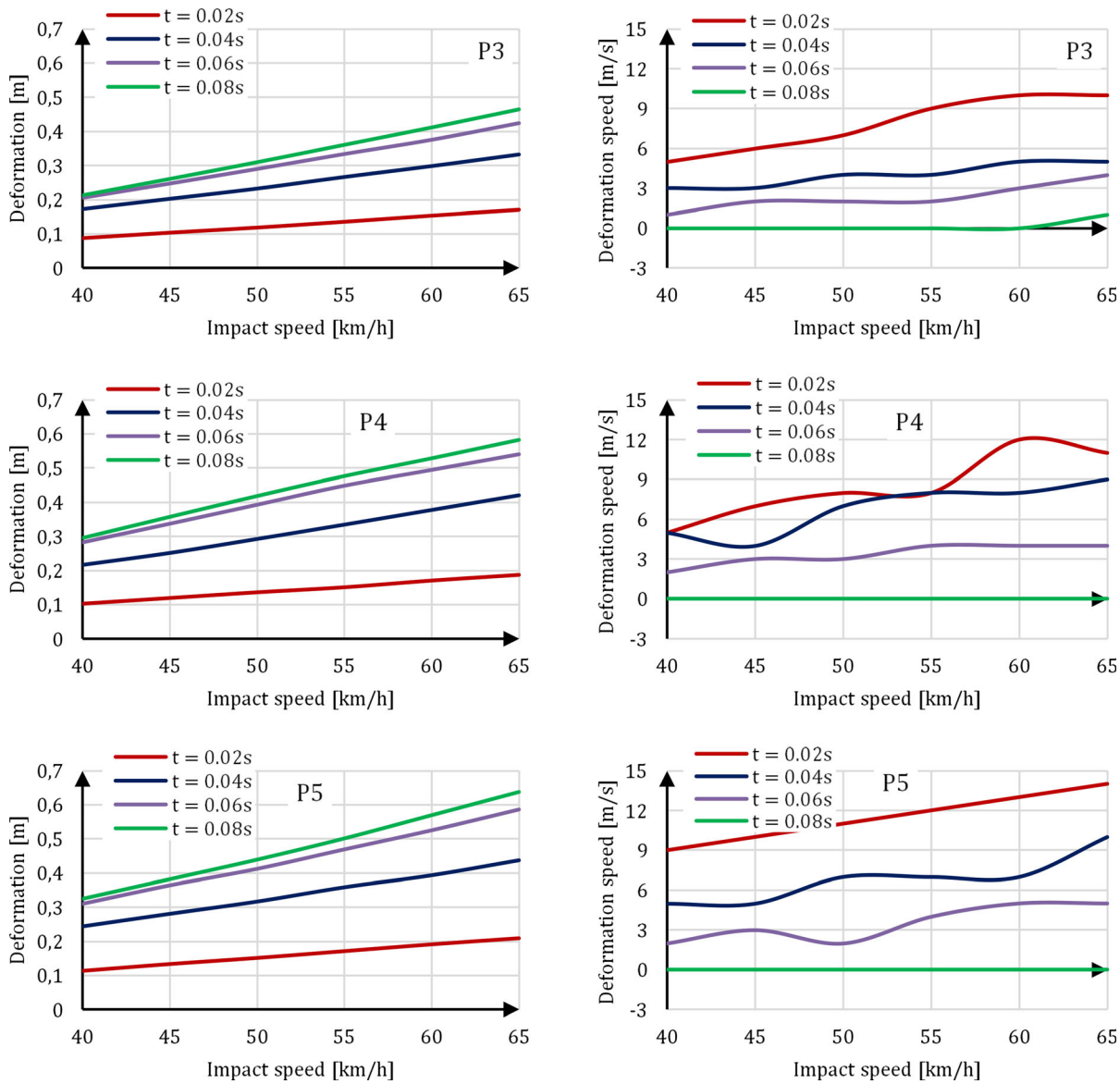

Fig. 18 Deformation and deformation rates of the car *B* body side as functions of the velocity of impact of car *A* (values at the instants of 0.02 s, 0.04 s, 0.06 s and 0.08 s from the beginning of the collision)

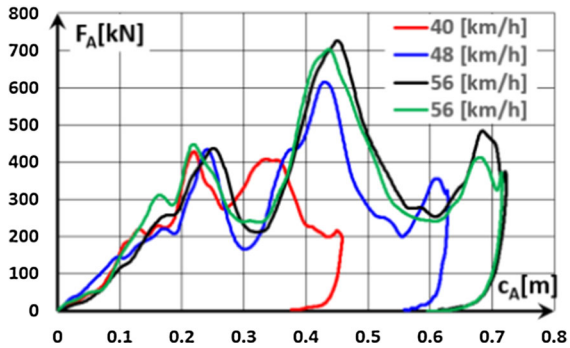

Fig. 19 Deformation characteristics $F_A(c_A)$ of the front of the Honda Accord car for various speeds of impact against a rigid barrier, based on results of NHTSA crash tests (Nos 5104, 5139, 5145, 5215 [17])

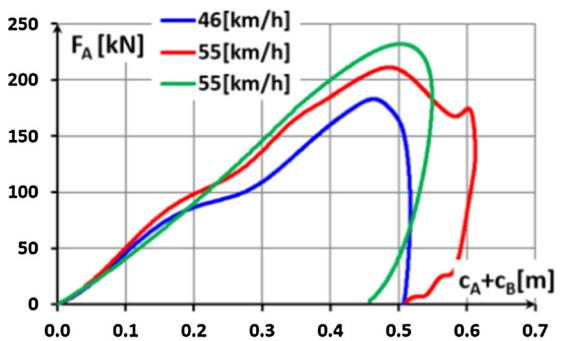

Fig. 20 Equivalent characteristic curves $F_A(c_A + c_B)$ for the front and side of the Honda Accord car (the Ł-PIMOT tests [10]

Compliance with ethical standards

Conflict of interest The authors declare that they have no conflict of interest.

Open Access This article is licensed under a Creative Commons Attribution 4.0 International License, which permits use, sharing, adaptation, distribution and reproduction in any medium or format, as long as you give appropriate credit to the original author(s) and the source, provide a link to the Creative Commons licence, and indicate if changes were made. The images or other third party material in this article are included in the article's Creative Commons licence, unless indicated otherwise in a credit line to the material. If material is not included in the article's Creative Commons licence and your intended use is not permitted by statutory regulation or exceeds the permitted use, you will need to obtain permission directly from the copyright holder. To view a copy of this licence, visit http://creativecommons.org/licenses/by/4.0/.

References

1. Stronge W.J. (2004) Impact Mechanics. Cambridge University Press 2004.
2. Laermann K-H (2015) Reflections on the correlation between mathematical and experimental analysis. Meccanica 50(4):887–891
3. Mazur JM (2006) Mathematical Models and the Experimental Analysis of Behavior. J Exp Anal Behav 85(2):275–291
4. Teng T-L, Chang K-C-H (2007) Development and validation of side-impact crash and sled testing finite-element models. Vehicle System Dynamics 45(10):925–937
5. Digges K., Eigen A. (2001) Measurements of vehicle compatibility in front-to-side crashes. Proceedings of the 2001 International IRCOBI Conference on the Biomechanics of Impact, Isle of Man, pp. 1–8.
6. Road traffic accidents in Poland in (2018) (2019) Polish Police Headquarters. Road Traffic Office, Warszawa, p 2019
7. Dong G, Wang D, Zhang J, Huang S (2007) Side structure sensitivity to passenger car crashworthiness during pole side impact. Tsinghua Science and Technology 9(18):290–295
8. Leone N, Kietlinski K, Unger M, Tijssens M (2015) Occupant protection performance in side impact collisions preceded by pre-crash deployment of on-board safety systems. 24 ESV Conference. Paper Number 15–0310:1–10
9. Velardocchia M, Unger M, Vigliani A, Leone N et al (2013) Integrated active and passive systems for a side impact scenario. SAE Technical Paper. https://doi.org/10.4271/2013-01-1162
10. Gidlewski M, Prochowski L, Jemioł L, Zardecki D (2019) The process of front-to-side collision of motor vehicles in terms of energy balance. Nonlinear Dyn 97(3):1877–1893
11. Prochowski L., Ziubinski M., Gidlewski M. (2018) Experimental and Analytic Determining of Changes in Motor Cars' Positions in Relation to Each Other During A Crash Test Carried Out to the FMVSS 214 Procedure. XI International Science-Technical Conference Automotive Safety, Slovakia, Publisher: IEEE, pp. 1–5.
12. Gilardi G, Sharf I (2002) Literature survey of contact dynamics modeling. Mech Mach Theory 37:1213–1239
13. Brach R. M., Brach R. M. (2005) Vehicle accident analysis and reconstruction methods. SAE International.
14. Huang, M. (2002) Vehicle crash mechanics. CRC Press LLC.
15. Elmarakbi A, Elkady M, El-Hage H (2013) Development of a new crash/dynamics control integrated mathematical model for crashworthiness enhancement of vehicle structures. Int J Crashworthiness 18(5):444–458
16. Brogliatto B. (2016) Nonsmooth Mechanics, Springer.
17. National Highway Traffic Safety Administration. Vehicle Crash Test Database, www.nhtsa.gov/research-data/databases-and-software.
18. Pawlus W, Karimi H, R., Robbersmyr K., G. (2014) Investigation of vehicle crash modeling techniques. Int J Adv Manuf Technol 70:965–993
19. Anderson R, W., G., Long A., D., Serre T. (2009) Phenomenological continuous contact–impact modeling for multibody simulations of pedestrian–vehicle contact

interactions based on experimental data. Nonlinear Dyn 58:199–208
20. Kubiak P, Siczek K, Dabrowski A, Szosland A (2016) New high precision method for determining vehicle crash velocity based on measurements of body deformation. Int J Crashworthiness 21:532–541
21. Nystrom GA (2001) Stiffness Parameters for Vehicle Collision Analysis, an Update. SAE Transactions Journal of Passenger Car Mechanical Systems Journal. 110(6):491–507
22. Gillardi G, Sharf I (2002) Literature survey of contact dynamics modeling. Mechanism and Machine Theory No 37:1213–1239
23. Pawlus W, Robbersmyr K, G., Karimi H., R. (2011) Mathematical modeling and parameters estimation of a car crash using data-based regressive model approach. Appl Math Model 35:5091–5107
24. Deb A, Srinivas K, C. (2008) Development of a new lumped parameter model for vehicle side-impact safety simulation. Proceedings of the Institution of Mechanical Engineers, Part D: Journal of Automobile Engineering 222:1793–1811
25. Viano D, Parentaeu C (2010) Severe-to-Fatal Injury Risks in Crashes With Two Front-Seat Occupants by Seat Belt Use. Traffic Inj Prev 11(3):294–299
26. Prochowski L., Gidlewski M., Ziubinski M., Dziewiecki K, (2019) The kinematics analysis of the body deformation process during frontal and lateral collision according to the FMVSS 214 procedure and classical test. Conference Paper. Abstracts, 15th Conference Dynamical Systems Theory and Applications, DSTA 2019, Lodz, 2019.
27. Mizuno K., Tateishi K., Arai Y., Nishimoto T. (2003) Research on vehicle compatibility in Japan. In Proceedings: International Technical Conference on the Enhanced Safety of Vehicles. National Highway Traffic Safety Administration. (Vol. 2003, pp. 12-p)
28. Harmati I, Várlaki P (2007) Identification of energy distribution for crash deformational processes of road vehicles. Acta Polytechnica Hungarica 4(2):19–28
29. Himmetoglu S., Yilmaz K.B., Yildirim B., Tekin A. (2018) Derivation of crush force versus deformation behaviour of vehicles at different impact speeds, Transport Means - Proceedings of the International Conference, 2018-October, pp. 49–56.
30. Kitagawa Y., Pal C. (2001) Evaluation of vehicle body stiffness and strength for car to car compatibility. SAE transactions, pp. 2348–2354.
31. Swanson J., Rockwell T., Beuse N. M., Summers L., Summers S., Park B. (2003) Evaluation of stiffness measures from the US new car assessment program. In Proceedings: International Technical Conference on the Enhanced Safety of Vehicles. National Highway Traffic Safety Administration. (Vol. 2003, pp. 13-p)
32. Nolan J. M., Lund A. K. (2001) Frontal offset deformable barrier crash testing and its effect on vehicle stiffness (No 2001–06–0109). SAE Technical Paper.
33. Wiacek C., Nagabhushana V., Rockwell T., Summers S., Zhao L., Collins L. A. (2015) Evaluation of frontal crash stiffness measures from the US New car assessment program. In ESV Conference, Seoul, South Korea.
34. Fuchs J. et al. (2019) Estimation of dynamic properties for the validation of driven railway vehicle models. The IAVSD International Symposium on Dynamics of Vehicles on Roads and Tracks. Springer, Cham, 2019.
35. Viehof M, Winner H (2018) (2018) Research methodology for a new validation concept in vehicle dynamics. Automotive and Engine Technology 3(1–2):21–27
36. Donlon JP, Poulard D, Lessley D, Riley P, Subit D (2015) Understanding how pre-impact posture can affect injury outcome in side impact sled tests using a new tool for visualization of cadaver kinematics. J Biomech 48(3):529–533
37. Tencer AF, Kaufman R, Mack Ch, Mock Ch (2005) Factors affecting pelvic and thoracic forces in near-side impact crashes: a study of US-NCAP, NASS and CIREN data. Accid Anal Prev 37(2):287–293
38. Yoganandan N, Pintar F, A, Stemper B. D., Gennarelli T. A., Weigel J. A. (2007) Biomechanics of side impact: Injury criteria, aging occupants and airbag technology. J Biomech 40(2):227–243

Publisher's Note Springer Nature remains neutral with regard to jurisdictional claims in published maps and institutional affiliations.